Dalton Transactions

PAPER

Cite this: *Dalton Trans.*, 2015, **44**, 6571

Challenges in the synthetic routes to $Mn(BH_4)_2$: insight into intermediate compounds†

Nikolay A. Tumanov,[a] Damir A. Safin,[a] Bo Richter,[b] Zbigniew Łodziana,[c] Torben R. Jensen,[b] Yann Garcia[a] and Yaroslav Filinchuk*[a]

Received 11th December 2014,
Accepted 10th February 2015

DOI: 10.1039/c4dt03807j

www.rsc.org/dalton

We have studied the reaction of $MnCl_2$ with MBH_4 (M = Li^+, Na^+, K^+) in Et_2O. Crystal structures of two new intermediates, named $[\{M(Et_2O)_2\}Mn_2(BH_4)_5]$ (M = Li^+, Na^+), were elucidated by X-ray diffraction. $Mn(BH_4)_2$ in a mixture with $LiBH_4$ or $NaBH_4$ forms upon the solvent removal in a vacuum. $[\{M(Et_2O)_2\}Mn_2(BH_4)_5]$ contains 2D layers formed by Mn and BH_4 groups, linked through the alkali metal atoms coordinated to Et_2O. The loss of the solvent molecules leads to the segregation of the partially amorphous or nanocrystalline $LiBH_4$/$NaBH_4$ and a creation of the 3D framework of the crystalline $Mn(BH_4)_2$. While using $LiBH_4$ led to $Mn(BH_4)_2$ contaminated with LiCl, presumably due to an efficient trapping of the latter salt by the $[Mn(BH_4)_2–Et_2O]$ system, the reaction with $NaBH_4$ produced chlorine-free $Mn(BH_4)_2$ accompanied with $NaBH_4$. Using KBH_4 led to the formation of $K_2Mn(BH_4)_4$ as a second phase. Two pyridine-containing solvomorphs, $[Mn(py)_3(BH_4)_2]$ and $[Mn(py)_4(BH_4)_2]\cdot 2py$, were isolated in pure form. However, $Mn(BH_4)_2$ partly decomposes upon removal of pyridine molecules.

Introduction

Borohydrides of alkali and alkali-earth metals are of interest as hydrogen storage materials, and they are even more intriguing as precursors to di-[1] or even trimetallic borohydrides[2] in order to tune the temperatures of dehydrogenation.[3,4] Up to now, monometallic borohydrides have been obtained by both solvent based and mechanochemical syntheses,[5] while mixed-metal borohydrides have usually been produced using mechanochemical synthesis.[6] Very recently it was found that the latter borohydrides can also be obtained in solutions.[7] Although borohydrides have been synthesized and characterized for many metals,[3,7–11] the synthesis of manganese borohydride, $Mn(BH_4)_2$, obtained *via* ball-milling of $MnCl_2$ with $LiBH_4$ in a 1 : 2 ratio, has been reported only recently.[12] The crystal structure of $Mn(BH_4)_2$ was successfully determined from powder X-ray diffraction data. However, the suggested mechanochemical approach suffers from the presence of significant amounts of LiCl, limiting the use of the resulting product.

Another route to $Mn(BH_4)_2$ is the metathesis reaction between $MnCl_2$ and alkaline borohydrides in Et_2O.[13,14] In particular, Schouwink *et al.* applied this method to obtain pure $Mn(BH_4)_2$ by reacting $MnCl_2$ and $LiBH_4$ in Et_2O (eqn (1)).[14]

$$MnCl_2 + 2LiBH_4 \rightarrow Mn(BH_4)_2 + 2LiCl \quad (1)$$

However, this approach was not reproducible – only one synthesis was reported to be successful, whereas other attempts failed due to the presence of LiCl in the final product. The same method was earlier applied by Černý *et al.* to obtain $Mg(BH_4)_2$, having a crystal structure similar to that of $Mn(BH_4)_2$.[15] However, the resulting product was also contaminated by LiCl, Li_2MgCl_4 and $LiBH_4$. Pure $Mg(BH_4)_2$ was obtained using the reaction of Et_3NBH_3 and MgH_2.[16,17] Because of the similarity between the structures, one may attempt to obtain pure $Mn(BH_4)_2$ by following the synthetic procedures to $Mg(BH_4)_2$. In particular, the latter borohydride can be obtained by reacting $MgBu_2$ either with $Al(BH_4)_3$ (eqn (2)) or $BH_3\cdot Me_2S$ (eqn (3)).[18,19] Applying both synthetic procedures to $Mn(BH_4)_2$ requires manganese dialkyl precursors, which are either highly unstable under ambient conditions[20] and/or commercially unavailable. Furthermore, the use of $Al(BH_4)_3$ is not practical because of its high instability and explosiveness.

$$3MgBu_2 + 2Al(BH_4)_3 \rightarrow 3Mg(BH_4)_2 + 2AlBu_3 \quad (2)$$

[a]*Institute of Condensed Matter and Nanosciences, Molecules, Solids & Reactivity (IMCN/MOST), Université Catholique de Louvain, Place L. Pasteur 1, 1348 Louvain-la-Neuve, Belgium. E-mail: yaroslav.filinchuk@uclouvain.be*

[b]*Center for Materials Crystallography (CMC), Interdisciplinary Nanoscience Center (iNANO), and Department of Chemistry, Aarhus University, Langelandsgade 140, DK-8000 Århus C, Denmark*

[c]*INP Polish Academy of Sciences, Department of Structural Research, ul. Radzikowskiego 152, 31-342 Kraków, Poland*

†CCDC 985621–985623. For crystallographic data in CIF or other electronic format see DOI: 10.1039/c4dt03807j

$$3MgBu_2 + 8H_3B{\cdot}SMe_2 \rightarrow 3Mg(BH_4)_2{\cdot}2Me_2S + 2BBu_3{\cdot}SMe_2 \quad (3)$$

With all these in mind, we have drawn our attention to obtain pure $Mn(BH_4)_2$ by synthesizing first its solvate, followed by removing solvent molecules from the structure. Unlike $Mn(BH_4)_2$, solvates of $Mg(BH_4)_2$ have been extensively studied.[18,19,21–23] These results are of importance as a guideline to manganese-containing derivatives because of the structural and property similarity of the corresponding analogues of Mn^{2+} and Mg^{2+} (salts, borohydrides, *etc.*).[24] Thus, we can suggest the same order of increasing donor strength of the solvent molecules for $Mn(BH_4)_2$ as it was found for $Mg(BH_4)_2$: Et_2O < THF < NH_2tBu ≈ piperidine < pyridine < benzylamine < DMSO.[21] In order to facilitate solvent removal from the structure as well as to avoid decomposition of the final $Mn(BH_4)_2$, the solvent molecules should be small and form weak interactions with the neighboring molecules in the structure. The last members of this series lack these properties and, hence, are unsuitable for our strategy. The most suitable solvents seem to be Et_2O and THF.

Makhaev *et al.* reported the synthesis of $Mn(BH_4)_2{\cdot}$THF, $NaBH_4{\cdot}Mn(BH_4)_2{\cdot}$3THF (solid), $Mn(BH_4)_2{\cdot}$2THF (yellow oil) and $Mn(BH_4)_2{\cdot}$3THF (solid).[25] The structure of the latter complex was established. However, it was found that $Mn(BH_4)_2{\cdot}$3THF transforms to $Mn(BH_4)_2{\cdot}$2THF, followed by the complete decomposition of manganese borohydride during heating.[26,27] This makes the THF solvates unsuitable for our approach.

In this work we report the synthesis of $Mn(BH_4)_2$ in Et_2O using $MnCl_2$ and MBH_4 (M = Li^+, Na^+, K^+) to examine the influence of the nature of the alkali metal on the purity of the final product. We also made a detailed study of intermediate compounds formed during the reaction. Results on using an even smaller dimethyl sulfide, Me_2S, as a solvent in synthesis of $Mn(BH_4)_2$ will be reported elsewhere.[28] It should be noted that the main difference in using Et_2O and Me_2S as reaction media is that the former solvent contains the "hard" oxygen donor atom, which is more suitable to efficiently solvate "hard" metal cations such as Li^+, Na^+ and K^+. The latter solvent, containing the "soft" sulfur donor atom, would efficiently solvate "soft" d-metal cation, *viz.* Mn^{2+}. Herein we present our results using the first, Et_2O-based, synthetic approach. This in-depth study will open an avenue for the synthesis of $Mn(BH_4)_2$. Furthermore, for comparison with the light Et_2O we also studied the reaction between $MnCl_2$ and $NaBH_4$ in a highly donor solvent, pyridine. Despite it allows one to isolate pure complexes of $Mn(BH_4)_2$, its desolvation leads to a partial decomposition of $Mn(BH_4)_2$.

Results and discussion

In agreement with Schouwink *et al.*,[14] as well as it was also established for $Mg(BH_4)_2$,[29] our numerous experiments revealed that the metathesis reaction between $MnCl_2$ and $LiBH_4$ in Et_2O (eqn (1)) was not reproducible to deliver pure $Mn(BH_4)_2$. Note, that this approach is based on the fact that both $MnCl_2$ and LiCl are poorly soluble in Et_2O, while $Mn(BH_4)_2$ is efficiently soluble in this solvent.

Our results demonstrate the formation of $Mn(BH_4)_2$, containing about 35 wt% of LiCl upon reacting $MnCl_2$ with $LiBH_4$ in Et_2O. We believe that, although LiCl is extremely poorly soluble in pure Et_2O (Table 1), it can be efficiently trapped by the [$Mn(BH_4)_2$–Et_2O] system, for example *via* formation of more complex intermediates, thus increasing the solubility. Another reason might come from the formation of very small particles of LiCl during the reaction, which cannot be filtered out even after using a PTFE membrane filter (22 μm pores).

Thus, using $LiBH_4$, as a borohydride source for the synthesis of $Mn(BH_4)_2$ in Et_2O, seems to be non-reliable due to the formation of LiCl, which significantly contaminates the resulting product. With this in mind, we have focused on alternative borohydride sources such as $NaBH_4$ and KBH_4. Both precursors, as well as NaCl and KCl, are much less soluble in Et_2O compared to the corresponding lithium analogues (Table 1). Thus, using $NaBH_4$ and KBH_4 increased the reaction time significantly. It is worth noting that before our investigations $LiBH_4$, being the most reactive alkali-metal borohydride, was the only source of borohydride to produce $Mn(BH_4)_2$. Thus, our studies on using both $NaBH_4$ and KBH_4 to react with $MnCl_2$ in solutions were challenging. However, one would expect similar reaction properties of $NaBH_4$ and KBH_4 as for $LiBH_4$ to produce $Mn(BH_4)_2$.

Slow evaporation of the solvent from the reaction mixture of $MnCl_2$ with MBH_4 (M = Li^+, Na^+, K^+) in Et_2O afforded yellow oil, which might be the result of the formation of mono- and/or polymetallic borohydrides with a high content of Et_2O. The

Table 1 Solubility of the reported compounds at 25 °C[a]

	LiCl	KCl	$LiBH_4$	$NaBH_4$	KBH_4	$MnCl_2$
Et_2O	0.77 mg/100 g[30] 0.6 mg/100 g[31]	—	1.4 M,[31] 7.53 wt%[32] 4.5 wt%[33]	Insoluble,[31,34] 0.02 g/100 g[35]	Insoluble[6]	Poorly soluble[36]
Dioxane	2.7 g/100 g[31]	—	—	—	—	Poorly soluble[36]
Pyridine	14.0 g/100 g[37] 10.0 g/100 g[38]	0.002 g l^{-1} (ref. 38)	—	3.4 g/100 g[39]	—	—
THF	4.3 g/100 g[40]	—	11.43 M,[31] 22.2 g/100 g[41]	0.07 g/100 g,[31] 0.1 g/100 g[39] 0.04 wt%[42]	Insoluble[6]	Soluble[36]

[a] No data were found for NaCl.

solvent molecules might both coordinate to the metal centers and serve as lattice solvents trapped within voids upon crystallization. Makhaev *et al.* reported that transition metal borohydrides form solvates with polyethers of the general formula $NaM^{n+}(BH_4)_{n+1}\cdot x$Solv (M = V, Fe, Mn; Solv = dimethoxyethane, bis(2-methoxyethyl) ether, THF).[43,44]

All our attempts to crystallize the collected oils in a glass capillary by cooling down to 100 K have failed. Further slow drying of these oils under vacuum yielded yellow crystalline materials. Crystals obtained in $NaBH_4$-based synthesis were suitable for single-crystal X-ray diffraction. According to single-crystal and powder X-ray diffraction data, materials formed from the $LiBH_4$- and $NaBH_4$-based syntheses are the corresponding dimetallic borohydride solvates $[\{M(Et_2O)_2\}Mn_2(BH_4)_5]$ (M = Li^+, sample Li_solv; Na^+, sample Na_solv). The bulk material of the Li_solv sample also contained LiCl. Further slow drying of these two samples led to the decomposition of dimetallic borohydrides with the formation of $Mn(BH_4)_2$ and the corresponding MBH_4 (M = Li^+, sample Li_dry; Na^+, sample Na_dry). However, only peaks for $Mn(BH_4)_2$ and LiCl, and $Mn(BH_4)_2$ and traces of $NaBH_4$ were found in the powder X-ray diffraction patterns of Li_dry and Na_dry, respectively. This might be explained by the complete, for M = Li^+, and partial for M = Na^+, amorphization of the released MBH_4, as well as by the very small size of the segregating MBH_4 particles. The KBH_4-based synthesis produced a mixture of $Mn(BH_4)_2$ and $K_2Mn(BH_4)_4$, with the latter compound being a minor product (~4 wt%) (sample K_dry). $K_2Mn(BH_4)_4$ has been previously obtained from the mechanochemical synthesis.[14] Thus, although 25% excess of $MnCl_2$ was used in the reactions with MBH_4 (M = Li^+, Na^+, K^+), a strong affinity to form bimetallic structures was observed in all three cases.

According to X-ray diffraction data, $[\{Li(Et_2O)_2\}Mn_2(BH_4)_5]$ and $[\{Na(Et_2O)_2\}Mn_2(BH_4)_5]$ crystallize in the monoclinic space groups *C*2/*c* and *C*2, respectively (Table 2). The volume of the unit cell differs by roughly a factor of two; however, the topology of the two structures is identical. Reconstruction of the reciprocal space sections for $[\{Na(Et_2O)_2\}Mn_2(BH_4)_5]$ did not show cell doubling in any direction, while the powder data for the Li-containing analogue clearly reveal superstructure peaks. The asymmetric unit in both compounds contains one Mn^{2+} cation, two BH_4^- anions in general positions and one on the 2 axis, one Et_2O molecule in a general position, and Li^+ or Na^+ cations in a special position. In both structures, each of the Mn^{2+} atoms coordinates four tetrahedral BH_4^- anions *via* edges with the formation of a slightly distorted $Mn(BH_4)_4$ tetrahedron. In the Li-containing compounds, the orientation of the BH_4^- groups cannot be reliably determined from the powder X-ray diffraction data. However, besides the orientation of the BH_4^- groups, other distances in the lithium structure can be determined quite precisely. The Mn–B bond distances are 2.280(7)–2.581(7) Å [2.329–2.497 Å; hereinafter the bond distances for the DFT-optimized structures are given in the brackets] and 2.403(11)–2.475(9) [2.383–2.452] Å in the Li- and Na-based structures, respectively. These values are comparable with those for pure $Mn(BH_4)_2$ and other compounds containing Mn^{2+} and BH_4^- fragments. Li^+ or Na^+ atoms are coordinated *via* edges to two BH_4^- groups with the Li–B and Na–B distances being 2.555(6) [2.582–2.566] and 2.700(11) [2.748] Å, respectively. Tetrahedral coordination spheres of Li^+ and Na^+ are further filled with two oxygen atoms from two Et_2O molecules with the Li–O and Na–O bond lengths 2.0030(14) [1.995–2.003] and 2.316(10) [2.377] Å, respectively. In both compounds, the BH_4^- group serves as a bridging ligand with respect to the two metal atoms, as in the solvent-free bimetallic borohydrides of transition metals (Zn^{2+}, Mn^{2+}, Sc^{3+}, Cd^{2+}, Y^{3+}).[1,14,45–50]

Since the positions of the hydrogen atoms are difficult to determine unambiguously from X-ray diffraction, we made DFT calculations on the experimental structures, clarifying the coordination modes of BH_4^- groups. Both compounds are insulators with a band gap of 2.1 and 1.9 eV for $[\{Li(Et_2O)_2\}Mn_2(BH_4)_5]$ and $[\{Na(Et_2O)_2\}Mn_2(BH_4)_5]$, respectively. Optimized structures clearly show bidentate coordination of all BH_4^- groups with respect to metal atoms in both compounds. The symmetry of the DFT-optimized structure of $[\{Li(Et_2O)_2\}Mn_2(BH_4)_5]$ is lower, the space group is *Cc* instead of *C*2/*c*. This happens due to small displacements of atoms, which do not change significantly the entire structure. Rietveld refinement in the space group *Cc* gives a good fit, but involves nearly twice as many refined parameters. Therefore, for the experimental structure we finally decided to keep the space group *C*2/*c*.

The Mn-based tetrahedra form 2D layers in the *bc* and *ac* planes for $[\{Li(Et_2O)_2\}Mn_2(BH_4)_5]$ and $[\{Na(Et_2O)_2\}Mn_2(BH_4)_5]$, respectively (Fig. 1). These 2D layers are linked through the Li- or Na-containing tetrahedra producing 3D structures (Fig. 1). Molecules of Et_2O are located between the 2D layers formed by Mn-based polyhedra (Fig. 1), which could explain the relatively

Table 2 Unit cell parameters of the reported compounds

	$[\{Li(Et_2O)_2\}Mn_2(BH_4)_5]$	$[\{Na(Et_2O)_2\}Mn_2(BH_4)_5]$	$[Mn(py)_3(BH_4)_2]$	$[Mn(py)_4(BH_4)_2]\cdot 2py$	$[Mg(py)_4(BH_4)_2]\cdot 2py$[22]
Space group	*C*2/*c*	*C*2	*C*2/*c*	*Ccca*	*Ccca*
Z	4	2	4	4	4
a/Å	21.7106(3)	14.5133(6)	12.3618(4)	11.516(2)	11.604(2)
b/Å	7.72944(12)	7.4487(3)	15.5064(5)	14.938(4)	15.114(2)
c/Å	14.02422(19)	10.7119(5)	9.2859(4)	17.263(8)	17.190(2)
β/°	110.8649(14)	104.338(5)	101.126(4)	90	90
V/Å^3	2199.09(6)	1121.96(9)	1746.53(11)	2970(2)	3014.7(7)
CCDC	985621	985622	985623		186648

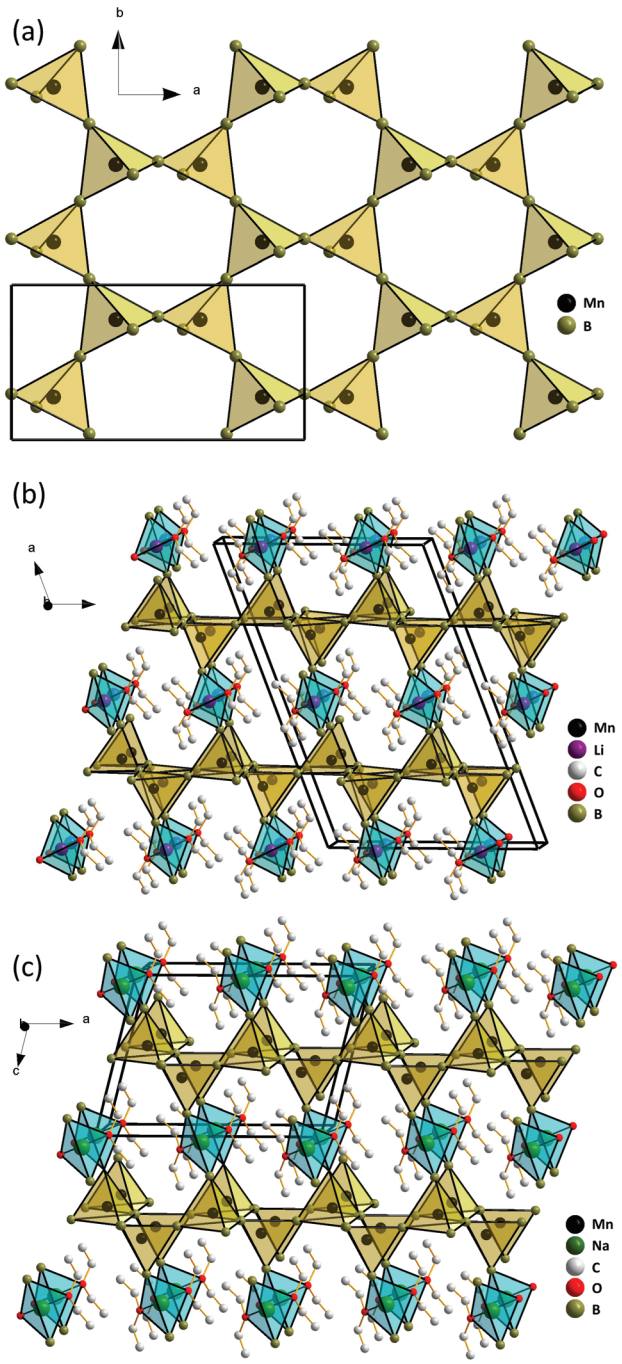

Fig. 1 The 2D layer formed by the MnB_4-based coordination tetrahedra in the structures of $[\{M(Et_2O)_2\}Mn_2(BH_4)_5]$ (M = Li^+, Na^+) (a). Crystal packing of $[\{Li(Et_2O)_2\}Mn_2(BH_4)_5]$ (b) and $[\{Na(Et_2O)_2\}Mn_2(BH_4)_5]$ (c). Polyhedra around the Mn atoms are shown in yellow, while those around the Li and Na atoms are given in blue. Hydrogen atoms were omitted.

easy release of the solvate molecules from the structures in a vacuum. The 2D layers formed by Mn-based polyhedra are almost the same in both structures, but the layers of alkali metal based polyhedra are different. In the structure of $[\{Na(Et_2O)_2\}Mn_2(BH_4)_5]$, all Na-based polyhedra are oriented in the same way, while in the structure of $[\{Li(Et_2O)_2\}Mn_2(BH_4)_5]$, the Li-based polyhedra alternate with two different orientations, which results in the double cell for this compound, compared to the Na-containing analogue. But even taking into account this difference, the structures remain topologically similar. A 2D honeycomb topology of the Mn-based tetrahedra suggests that the magnetic ordering might be complex at low temperatures.[51] But magnetic ordering cannot be directly detected by X-ray diffraction, and it is not present at the temperatures of interest – thus it is unrelated to the present study.

We suggest that evaporation of the molecules of Et_2O breaks the coordination environment around the Li^+ or Na^+ atoms, leading to a collapse of the structure with the formation of $Mn(BH_4)_2$ and corresponding MBH_4 (M = Li^+, Na^+).

The Raman spectra of Li_solv, Li_dry, Na_dry and K_dry (Fig. 2) contain characteristic bands for the BH_4^- groups, seen also in the structure of $Mn(BH_4)_2$.[16] Furthermore, the Raman spectrum of Li_solv exhibits a set of characteristic bands for the Et_2O molecules: medium bands at 1360 and 1450 cm^{-1} as well as number of intense bands at 2820–3020 cm^{-1}, corresponding to the CH vibrations of the ethyl groups; and a weak band at about 1090 cm^{-1}, which is typical for the COC asymmetric stretches. It should be noted that no bands for the Et_2O molecules were found in the Raman spectra of Li_dry, Na_dry and K_dry testifying the complete evaporation of the solvent molecules.

The thermal properties of Li_solv, Li_dry, Na_dry and K_dry under an argon atmosphere were studied by means of the TG analysis (Fig. 3). Li_solv is stable up to about 35 °C and decomposes in three clearly (despite the mass drift) defined steps. The first remarkable step up to about 110 °C corresponds to the evolution of Et_2O. The second mass loss up to about 160 °C is due to the decomposition of $Mn(BH_4)_2$.[28,52] It should be noted that this decomposition step was found in the TG data of all compounds (Fig. 3). However, the temperature-dependent *in situ* powder X-ray diffraction data, collected for Li_solv, exhibit peaks exclusively for LiCl after about 105 °C accompanied with the new very broad humps due to the formation of the either amorphous or liquid phase containing

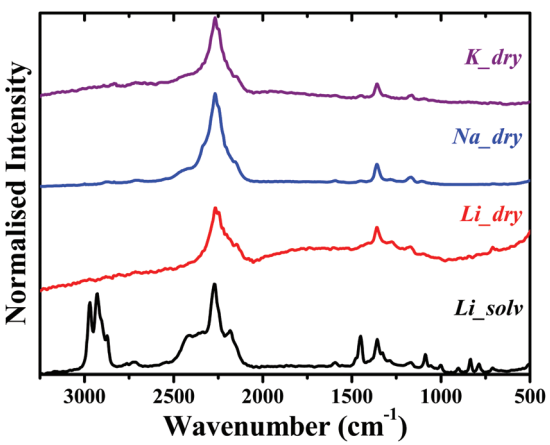

Fig. 2 Raman spectra of Li_solv, Li_dry, Na_dry and K_dry. The spectrum of Na_solv is similar to that of Li_solv.

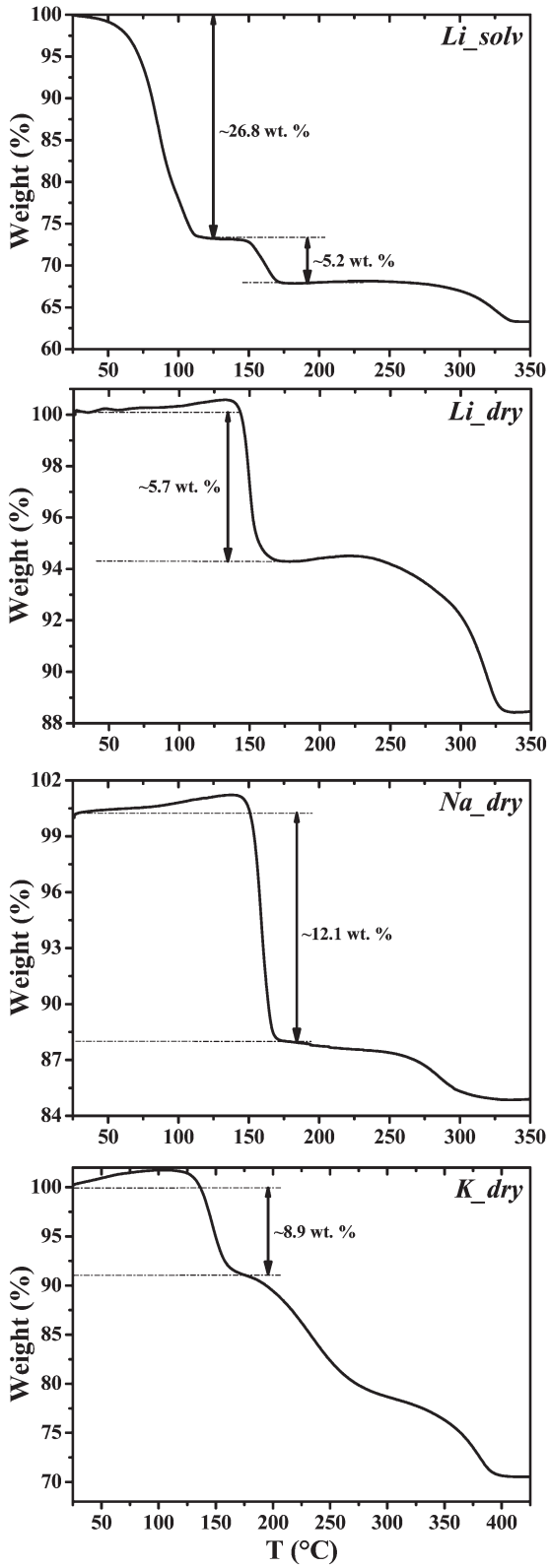

Fig. 3 TG analyses of Li_solv, Li_dry, Na_dry and K_dry performed under a dynamic argon atmosphere. The TG data for Na_solv are similar to those of Li_sov. All mass loss steps were found to be endothermic.

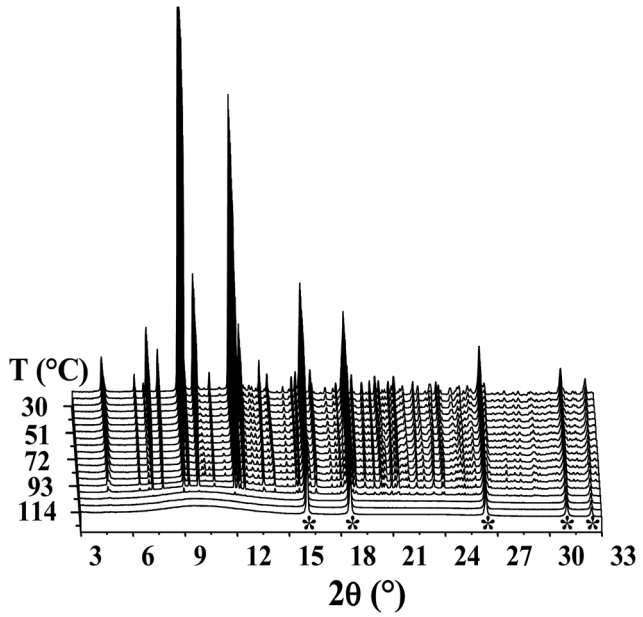

Fig. 4 *In situ* synchrotron X-ray diffraction on Li_solv measured from 30 to 130 °C (λ = 0.82742 Å). [{Li(Et$_2$O)$_2$}Mn$_2$(BH$_4$)$_5$] decomposes at about 105 °C. Peaks from the LiCl phase are marked with asterisks.

dissolved Mn(BH$_4$)$_2$ and LiBH$_4$ (Fig. 4). The observed discrepancies between the TG and powder X-ray diffraction data might be explained by different experimental conditions. In particular, the latter experiments were done in a capillary sealed by wax, which can be considered as a "closed" system, while TG studies were performed in a crucible under a flow of argon, thus, in an "open" system. The latter system favors an efficient removal of the evaporated Et$_2$O, while it is blocked in the former system. This, in turn, leads to dissolving of the crystalline borohydride residues, released during the decomposition (Table 1). However, LiCl remains intact under applied experimental conditions due to its, first, poor solubility in Et$_2$O (Table 1) and, second, high thermal stability.

The TG for Li_dry is very similar to that of Li_solv after the latter compound completely losses Et$_2$O (Fig. 3). The TG data for Na_dry and K_dry, with the first step of mass loss due to the decomposition of Mn(BH$_4$)$_2$, show the same features as Li_dry (Fig. 3). However, since the sample K_dry contains also K$_2$Mn(BH$_4$)$_2$, its TG is, obviously, complicated by the decomposition pathway of this bimetallic borohydride.[14]

Various solvates of the same borohydride could be used to produce new polymorphs. In particular, porous polymorphs, which are even more promising for gas storage. For example, porous γ-Mg(BH$_4$)$_2$ was successfully obtained from the Mg(BH$_4$)$_2$·0.5Me$_2$S solvate.[19] However, the formation of a stable borohydride from its solvate requires that the parent structure comprises a rigid 3D framework formed by coordination polyhedra around the metal atoms, or at least the presence of rigid 3D fragments. As we described above, both dimetallic solvates exhibit exclusively 2D Mn-BH$_4$ layers. The loss of the solvent molecules leads to the segregation of the partially amorphous or nanocrystalline LiBH$_4$/NaBH$_4$ and the

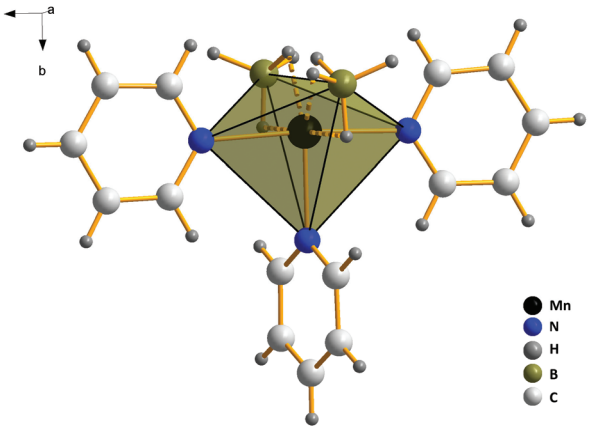

Fig. 5 Molecular structure of $[Mn(py)_3(BH_4)_2]$.

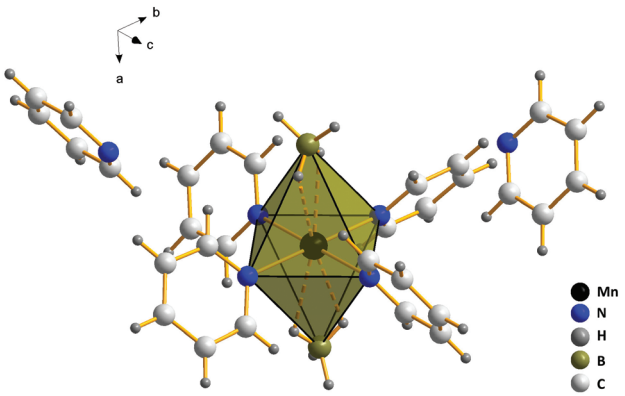

Fig. 6 Molecular structure of $[Mn(py)_4(BH_4)_2]\cdot 2py$.

creation of the new 3D framework of the crystalline $Mn(BH_4)_2$. The behaviour of the mononuclear pyridine complexes of $Mn(BH_4)_2$, obtained in this work, illustrates that the formation of stable borohydrides from their solvates is difficult in the absence of rigid metal-borohydride frameworks present already in the parent structure.

The reaction of $MnCl_2$ with $NaBH_4$ in pyridine produces at least two solvates, $[Mn(py)_3(BH_4)_2]$ and $[Mn(py)_4(BH_4)_2]\cdot 2py$. According to single-crystal X-ray diffraction data the former complex crystallizes in the monoclinic $C2/c$ space group and exhibits a heteroleptic mononuclear complex (Fig. 5 and Table 2). The asymmetric unit contains one BH_4^- anion, one molecule of pyridine in general and one in special positions, and one Mn^{2+} cation on the 2-fold axis, which results in a molecular complex with the C_2 symmetry. The Mn^{2+} atom coordinates two tetrahedral BH_4^- anions *via* the edges at Mn–B distances of 2.483(2) Å. The coordination sphere of the metal center is completed by three nitrogen atoms from three pyridine molecules. The Mn–N bond distances are 2.246(3) and 2.2823(19) Å. The coordination environment of Mn can be described either as square-pyramidal or trigonal bipyramidal depending on the parameter $\tau = (\beta - \alpha)/60$, where α and β are the two largest bond angles around the metal ion. An ideal square pyramidal arrangement is described by the value of $\tau = 0$, while an ideal trigonal bipyramidal arrangement has the value of $\tau = 1$.[53] The largest bond angles in the coordination sphere of Mn^{2+} are 175.92(8) and 127.72(11)°. This gives τ value of 0.8, which is significantly closer to that of the ideal trigonal bipyramidal around the metal atom. The equatorial plane of the bipyramid is formed by both BH_4^- anions and one of the pyridine molecules.

Unfortunately, we were unable to obtain single crystals of $[Mn(py)_4(BH_4)_2]\cdot 2py$ suitable for structure determination. However, we were successful in determining the space group and the unit cell parameters. Based on the obtained data, we suggest that $[Mn(py)_4(BH_4)_2]\cdot 2py$ is isostructural to the previously reported complex $[Mg(py)_4(BH_4)_2]\cdot 2py$[21] (Table 2). Thus, the manganese derivative comprises a discrete heteroleptic mononuclear complex $[Mn(py)_4(BH_4)_2]$ and two lattice pyridine molecules (Fig. 6). The Mn^{2+} cation coordinates four pyridine molecules and two BH_4^- anions forming a distorted octahedron.

Both pyridine-containing solvomorphs contain mononuclear Mn complexes, which are well isolated from each other. The departure of the solvent molecules leads to a complete structural rearrangement accompanied by $Mn(BH_4)_2$ decomposition and gas release. The structures contain no polymeric chains to form relatively stable frameworks, and they turned out to be unsuitable as precursors for obtaining neither porous nor even dense $Mn(BH_4)_2$ polymorphs. However, both pyridine complexes described in this work, as well as the previously reported magnesium analogue,[22] are an intriguing starting point for the possible formation of porous metal organic borohydride frameworks using polypyridine ligands as organic linkers aiming for different topologies and porosity, like for example described in the work of Ingleson *et al.*[54]

Conclusions

In summary, we have studied the synthetic pathway to $Mn(BH_4)_2$ by reacting $MnCl_2$ and alkali metal borohydrides in diethyl ether. The two new solid intermediates $[\{M(Et_2O)_2\}Mn_2(BH_4)_5]$ ($M = Li^+$, Na^+) were isolated and characterized. We found that pure $Mn(BH_4)_2$ could not be obtained by this approach because of the inclusion of $LiBH_4$ or $NaBH_4$ leading to the stable bimetallic solvates that were isolated from the reaction mixture. Moreover, using $LiBH_4$ is less favorable due to the efficient trapping of LiCl by the $[Mn(BH_4)_2–Et_2O]$ system. Using $NaBH_4$ allows one to obtain $Mn(BH_4)_2$ with some of the starting borohydride, while KBH_4 leads to $Mn(BH_4)_2$ contaminated by $K_2Mn(BH_4)_4$.

We have also obtained two new pyridine solvates of $Mn(BH_4)_2$, by reacting $MnCl_2$ with $NaBH_4$ in pyridine. Both solvomorphs consist of mononuclear complexes of Mn, that are not suitable as precursors for pure $Mn(BH_4)_2$, as it partly decomposes upon removal of pyridine molecules.

Experimental

Materials

All experiments were performed under anhydrous conditions using Schlenk techniques and argon as a protecting gas. All materials were used as received and without further purification: $MnCl_2$ (Sigma-Aldrich, anhydrous, 99.99%), $LiBH_4$ (Sigma-Aldrich, ≥95%), $NaBH_4$ (Alfa Aesar, ≥97%), (Sigma-Aldrich, ≥99.9%), Et_2O (VWR, H_2O < 11 ppm), pyridine (Sigma-Aldrich, anhydrous, 99.8%).

Analytical methods

Raman spectra were recorded using a FTIR Nicolet Magna 860 with a Raman unit and a Nd:YVO_4 (λ = 1064 nm) laser. Samples were placed in glass capillaries under an inert atmosphere and sealed with vacuum grease. Thermogravimetric analysis was done using a SDT 2960 Simultaneous DTA-TGA instrument under a dynamic argon atmosphere (100 mL min^{-1}) from ambient temperature to 600 °C with a 5 °C min^{-1} heating rate.

Synthesis

Reaction of $MnCl_2$ with $LiBH_4$ in Et_2O. A pink suspension of $MnCl_2$ (2.52 g, 20.0 mmol) and $LiBH_4$ (0.70 g, 32.0 mmol) in Et_2O (120 mL) was vigorously stirred for about 24 h. The resulting mixture was filtered using first a microporous glass filter and then the PTFE membrane filter (22 μm pores). The filtrate was slowly (~2 h) concentrated in a vacuum at room temperature. During concentration, a fine crystalline white powder of LiCl was precipitated alongside with the formation of pale yellow oil. Further concentration yielded a pale yellow solid material (sample Li_solv, sample designations and phase content are summarized in Table 3), which was characterized, according to the powder X-ray diffraction data, as a mixture of $[\{Li(Et_2O)_2\}Mn_2(BH_4)_5]$ (79.4 wt%) and LiCl (20.6 wt%). The solid material was further dried in a vacuum at room temperature for about 2.5 days. The resulting pale yellow powder (sample Li_dry in Table 3) was characterized, according to the powder X-ray diffraction data, as a mixture of $Mn(BH_4)_2$ (65 wt%) and LiCl (35 wt%). Based on the composition of the initial sample, the final product should contain $Mn(BH_4)_2$ (61.5 wt%), LiCl (30.7 wt%) and $LiBH_4$ (7.9 wt%). However, the powder X-ray diffraction pattern did not exhibit peaks for $LiBH_4$, which is, probably, due to the amorphization of the latter compound or due to very small size of its particles.

Reaction of $MnCl_2$ with $NaBH_4$ in Et_2O. A pink suspension of $MnCl_2$ (2.52 g, 20.0 mmol) and $NaBH_4$ (1.21 g, 32.0 mmol) in Et_2O (120 mL) was vigorously stirred for several days until a clear yellow solution with white precipitate appeared. The reaction proceeded much slower than the analogous reaction with $LiBH_4$ due to the lower solubility of $NaBH_4$ in Et_2O. The resulting mixture was filtered using a microporous glass filter. The filtrate was slowly concentrated and the formation of pale yellow oil was observed. Further slow drying of this oil in a vacuum at room temperature resulted in yellow crystals (sample Na_solv in Table 3), according to the single-crystal and powder X-ray diffraction data, of $[\{Na(Et_2O)_2\}Mn_2(BH_4)_5]$. The solid material was further dried in a vacuum at room temperature for about 2.5 days. The resulting pale yellow powder (sample Na_dry in Table 3) was characterized, according to the powder X-ray diffraction data, as a mixture of $Mn(BH_4)_2$ (94 wt%) and $NaBH_4$ (6 wt%). Based on the composition of the initial sample, the final product should contain about 30.9 wt% of $NaBH_4$. The observed discrepancy is, most likely, due to a partial amorphization of $NaBH_4$ or due to very small size of its particles.

Reaction of $MnCl_2$ with KBH_4 in Et_2O. A pink suspension of $MnCl_2$ (2.52 g, 20.0 mmol) and KBH_4 (1.73 g, 32.0 mmol) in Et_2O (120 mL) was vigorously stirred for several days until a clear yellow solution with white precipitate appeared. The reaction proceeded much slower than the analogous reaction with $LiBH_4$ due to the lower solubility of KBH_4 in Et_2O. The resulting mixture was filtered using a microporous glass filter. The filtrate was slowly concentrated and the formation of pale yellow oil was observed. Further slow drying of this oil in a vacuum at room temperature resulted in a pale yellow solid, which was further dried in a vacuum at room temperature for about 2.5 days. The resulting pale yellow powder (sample K_dry in Table 3) was characterized, according to the powder X-ray diffraction data, as a mixture of $Mn(BH_4)_2$ (96 wt%) and $K_2Mn(BH_4)_4$ (4 wt%).

Reaction of $MnCl_2$ with $NaBH_4$ in pyridine. A dark brown suspension of $MnCl_2$ (2.52 g, 20.0 mmol) and $NaBH_4$ (1.21 g, 32.0 mmol) in pyridine (py, 120 mL) was vigorously stirred for two days. The resulting mixture was filtered using the PTFE membrane filter (22 μm pores). The filtrate was slowly concentrated in a vacuum at room temperature until colorless crystals were formed. These crystals were stable in the mother liquor at room temperature for few hours, but quickly decomposed at room temperature when isolated from the solution, even under inert conditions. At least two pyridine-containing compounds, $[Mn(py)_3(BH_4)_2]$ and $[Mn(py)_4(BH_4)_2]\cdot 2py$, were obtained, according to the single-crystal X-ray diffraction data.

Table 3 Phase composition of samples

Sample name	Phases	wt%, experimental X-ray data	wt%, calculated from the initial composition
Li_solv	$[\{Li(Et_2O)_2\}Mn_2(BH_4)_5]$	79.4	—
	LiCl	20.6	
Li_dry	$Mn(BH_4)_2$	65	61.5
	$LiBH_4$	0	7.9
	LiCl	35	30.7
Na_solv	$[\{Na(Et_2O)_2\}Mn_2(BH_4)_5]$	100	—
Na_dry	$Mn(BH_4)_2$	94	69.1
	$NaBH_4$	6	30.9
K_dry	$Mn(BH_4)_2$	96	—
	$K_2Mn(BH_4)_4$	4	

Single crystal X-ray crystallography

The X-ray data were collected at 150(2) K on a MAR345 image plate detector using Mo Kα radiation (Rigaku UltraX 18 rotation anode, Xenocs Fox3D focusing multilayer mirror). The

data were integrated using the CrysAlisPro software.[55] The implemented multi-scan absorption correction was applied. The structures were solved by direct methods using the SHELXS-97[56] program and refined by full-matrix least squares on $|F|^2$ using SHELXL-97.[56] Non-hydrogen atoms were refined anisotropically, while hydrogen atoms of Et_2O were localized from a differential Fourier map, but were placed at calculated positions in a riding mode with temperature factors fixed at 1.2 times U_{eq} of the parent atoms and 1.5 times U_{eq} for the methyl groups. The B–H and H–H distances in the BH_4 groups were constrained to form ideal tetrahedrons. Inspection of the differential Fourier map revealed the presence of positional disorder in Et_2O. Attempts to model this disorder with several positions of the Et_2O molecule resulted in an insignificant improvement of the model, so we modeled the disorder with one position, but with higher atomic displacements.

Synchrotron powder X-ray crystallography

The synchrotron radiation powder X-ray diffraction data were collected at the Swiss–Norwegian beamline BM1A at the European Synchrotron Radiation Facility (ESRF) (Grenoble, France) using a PILATUS 2M pixel detector. The wavelength was 0.82742 Å, and the sample-to-detector distance was 430 mm. These parameters along with image plate tilt angles were calibrated using a standard LaB_6 sample. The Li_solv sample was sealed in a thin-walled glass capillary under an argon atmosphere and measured at 100(2) K. Two-dimensional diffraction images from this sample were integrated using the ESRF Fit2D program.[57] The pattern was indexed using DICVOL04[58] in a centered monoclinic crystal system. Analysis of systematic absences suggested the *C*2/*c* and *Cc* space groups. Based on the assumed composition, $Mn(BH_4)_2{\cdot}x(C_2H_5)_2O$, and an approximate volume of the $Mn(BH_4)_2$ unit being 113 Å^3, and the volume of the Et_2O molecule being 125 Å^3, we suggested the composition of $3Mn(BH_4)_2{\cdot}2Et_2O$. However, attempts to solve the structure applying this composition by global optimization in direct space in the FOX[59] program failed. The occupancy of all but one Mn atoms was close to 0. Therefore, we suggested the presence of Li atoms along with Mn in the structure. The structure was finally solved and refined in the *C*2/*c* space group with a composition of $[\{Li(Et_2O)_2\}Mn_2(BH_4)_5]$. In the final refinement, antibump restraints were 3 Å for the O–O and B–O contacts, 1.8 Å for O–H, 2.8 Å for B–C and Mn–C, 2.2 Å for H–H, and of 3.3 Å for B–B distances. The final refinement was done with the *C*2/*c* space group using the Rietveld method in the Fullprof suite software.[60] Coordinates of the Et_2O molecule were refined, with its orientation and configuration being fixed. The bond lengths in the Et_2O and BH_4 groups were constrained to be close to the following values: d(C–C) 1.50 Å, d(C–O) 1.425 Å, $d(C–H)_{CH3}$ 0.97 Å, $d(C–H)_{CH2}$ 0.96 Å, d(B–H) 1.13 Å, $d(H–H)_{BH4}$ 1.841 Å. The bond angles were constrained using soft distance and angle constraints. The torsion angles of the CH_3 groups in Et_2O were constrained using distance constraints to prevent an eclipsed conformation. One of the BH_4 groups was found on the inversion center, and this group was disordered over two 50/50% orientations since the symmetry of the BH_4 group is incompatible with an inversion center. The orientation of this group was constrained using distance restrains to make all Mn–H distances equal. Overall, 52 distance constraints and 25 angle constraints were applied. The second phase, LiCl, was modeled, with a final weight fraction of 20.54(10)%. The background was described by a linear interpolation of the selected points. The final discrepancy factors were: R_B = 5.05%, R_F = 6.30%, R_p = 10.52% and R_{wp} = 11.29%. The refinement profile is shown in Fig. 7.

Laboratory powder X-ray crystallography

Powder X-ray diffraction data were collected on a MAR345 image plate detector using Mo Kα radiation (Rigaku UltraX 18 rotation anode, Xenocs Fox3D focusing multilayer mirror). The two-dimensional diffraction images were integrated using the ESRF Fit2D[56] program. The integrated patterns were treated using the Fullprof suite software.[60]

DFT calculations

The structures were optimized by a conjugated gradient method within plane wave formulation of spin polarized density functional theory (DFT).[61] The electronic configuration of $1s^22s^1$ for Li, $2p^63s^1$ for Na, $3d^64s^1$ for Mn, $2s^22p^2$ for C, $2s^22p^4$ for O, $2s^22p^1$ for B, and $1s^1$ for H was represented by projected augmented wave potentials.[62] The gradient corrected (GGA) functional[63] was applied. The initial structure from the Rietveld refinement was optimized with respect to the internal atomic positions, the unit cell shape and volume were fixed. The on-site Coulomb repulsion[64] U = 4 was applied to the manganese d electrons. Since the manganese atoms are arranged in honeycomb-like 2D networks (Fig. 1) the ground state magnetic ordering could be nontrivial. This is despite the fact of obvious antiferromagnetic superexchange interaction between each adjacent Mn^{2+} linked by the BH_4^- anion. For example the lowest energy state with a collinear antiferro-

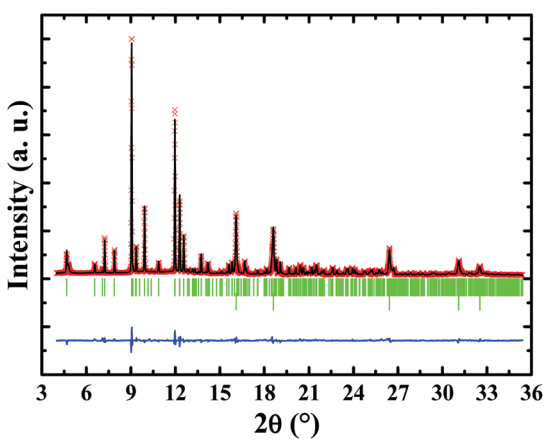

Fig. 7 Rietveld refinement plot for $[\{Li(Et_2O)_2\}Mn_2(BH_4)_5]$. Red crosses and black line show the experimental and calculated data, respectively. Blue line is the difference profile, and green marks indicate Bragg positions.

magnetic arrangement of sub-layers with up and down oriented BH_4^- tetrahedra is only 110 and 118 meV per formula unit more stable than the ferromagnetic one for $[\{Li(Et_2O)_2\}Mn_2(BH_4)_5]$ and $[\{Na(Et_2O)_2\}Mn_2(BH_4)_5]$, respectively. Moreover, it does not affect the structural configuration of the light atoms in the lattice. Noncollinear ordering of the magnetic moments requires larger superstructures, but around the room temperature they will not be present. We have checked that the total ground state energy for noncollinear spin arrangement varies on the scale of single or tenth of meV. Interestingly, in both compounds Mn formally is in the oxidation state 2+, however it is tetrahedrally coordinated by four BH_4^- anions. This coordination environment enforces a high spin arrangement of the Mn d-electrons. The calculated magnetic moments of Mn are $4.33\mu_B$ for the ferromagnetic, and ±4.29 or $\pm4.28\mu_B$ for the antiferromagnetic orders in $[\{Li(Et_2O)_2\}Mn_2(BH_4)_5]$ and $[\{Na(Et_2O)_2\}Mn_2(BH_4)_5]$, respectively. In order to avoid complications related to the fact that numerical values of the magnetic moments depend on particular choice of the Hubbard U,[65] the possibility of induction of the dipole moments/ferroelectricity due to noncentrosymmetry, noncollinear spin arrangements on the honeycomb lattices[51] overall resulting in exotic magnetic configurations, the antiferromagnetic ordering of Mn magnetic moments, as described above, was assumed. The crystal structures are almost the same regardless of the ferro and antiferro spin ordering. Each system was relaxed until forces exerted on atoms were below 0.01 eV A^{-1}. For $[\{Li(Et_2O)_2\}Mn_2(BH_4)_5]$ with a static disorder of BH_4^- groups two different ordered configurations of BH_4^- were assumed. The above mentioned assumptions are sources of errors; however we do not expect them to be larger than ~0.1 eV per formula unit, and they are of minor importance for the crystal structure.

CCDC 985621 ($[\{Li(Et_2O)_2\}Mn_2(BH_4)_5]$), 985622 ($[\{Na(Et_2O)_2\}Mn_2(BH_4)_5]$) and 985623 ($[Mn(py)_3(BH_4)_2]$) contain the supplementary crystallographic data. DFT optimized structures of $[\{Li(Et_2O)_2\}Mn_2(BH_4)_5]$ and $[\{Na(Et_2O)_2\}Mn_2(BH_4)_5]$ are available as ESI.†

Acknowledgements

The authors acknowledge FNRS (CC 1.5169.12, PDR T.0169.13, EQP U.N038.13) for financial support. We acknowledge the Fonds Spéciaux de Recherche (UCL) for the incoming postdoctoral fellowship co-funded by the Marie Curie actions of the European Commission granted to N. A. Tumanov and WBI (Belgium) for the postdoctoral position allocated to D. A. Safin. We thank ESRF for the beamtime allocation at the SNBL and V. Dyadkin for help, and A. Railliet for the help with thermogravimetric measurements. Part of this work was supported by the COST Action MP1103 "Nanostructured materials for solid-state hydrogen storage", by the Danish Council for Strategic Research, *via* the research project HyFillFast, the Danish National Research Foundation, Center for Materials Crystallography (DNRF93), and by the Danish Research Council for Nature and Universe (Danscatt). We acknowledge funding from the European Community's Seventh Framework Programme, the Fuel Cells and Hydrogen Joint Undertaking (FCH JU), project BOR4STORE (303428). We are grateful to the Carlsberg Foundation for support. Z. Łodziana acknowledges CPU allocation at the PLGrid Infrastructure and support by a grant from Switzerland through the Swiss Contribution to the enlarged European Union.

Notes and references

1 D. Ravnsbaek, Y. Filinchuk, Y. Cerenius, H. J. Jakobsen, F. Besenbacher, J. Skibsted and T. R. Jensen, *Angew. Chem., Int. Ed.*, 2009, **48**, 6659.
2 R. Černý, P. Schouwink, Y. Sadikin, K. Stare, L. Smrčok, B. Richter and T. R. Jensen, *Inorg. Chem.*, 2013, **52**, 9941.
3 L. H. Rude, T. K. Nielsen, D. B. Ravnsbaek, U. Bösenberg, M. B. Ley, B. Richter, L. M. Arnbjerg, M. Dornheim, Y. Filinchuk, F. Besenbacher and T. R. Jensen, *Phys. Status Solidi A*, 2011, **208**, 1754.
4 Y. Nakamori, K. Miwa, A. Ninomiya, H. Li, N. Ohba, S. Towata, A. Züttel and S. Orimo, *Phys. Rev. B: Condens. Matter*, 2006, **74**, 045126.
5 H. Hagemann and R. Cerný, *Dalton Trans.*, 2010, **39**, 6006.
6 J. Huot, D. B. Ravnsbæk, J. Zhang, F. Cuevas, M. Latroche and T. R. Jensen, *Prog. Mater. Sci.*, 2013, **58**, 30.
7 T. Jaroń, P. A. Orłowski, W. Wegner, K. J. Fijałkowski, P. J. Leszczyński and W. Grochala, *Angew. Chem., Int. Ed.*, 2015, **54**, 1236.
8 Y. Filinchuk, D. Chernyshov and V. Dmitriev, *Z. Kristallogr.*, 2008, **223**, 649.
9 M. B. Ley, L. H. Jepsen, Y.-S. Lee, Y. W. Cho, J. M. Bellosta von Colbe, M. Dornheim, M. Rokni, J. O. Jensen, M. Sloth, Y. Filinchuk, J. E. Jørgensen, F. Besenbacher and T. R. Jensen, *Mater. Today*, 2014, **17**, 122.
10 F. Pendolino, *J. Phys. Chem. C*, 2012, **116**, 1390.
11 L. H. Jepsen, M. B. Ley, Y.-S. Lee, Y. W. Cho, M. Dornheim, J. O. Jensen, Y. Filinchuk, J. E. Jørgensen, F. Besenbacher and T. R. Jensen, *Mater. Today*, 2014, **17**, 129.
12 R. Černý, N. Penin, H. Hagemann and Y. Filinchuk, *J. Phys. Chem. C*, 2009, **113**, 9003.
13 G. Monnier, *Ann. Chim.*, 1957, **13**, 14.
14 P. Schouwink, V. D'Anna, M. B. Ley, L. M. Lawson Daku, B. Richter, T. R. Jensen, H. Hagemann and R. Černý, *J. Phys. Chem. C*, 2012, **116**, 10829.
15 R. Cerný, Y. Filinchuk, H. Hagemann and K. Yvon, *Angew. Chem., Int. Ed.*, 2007, **46**, 5765.
16 Y. Filinchuk, R. Černý and H. Hagemann, *Chem. Mater.*, 2009, **21**, 925.
17 K. Chłopek, C. Frommen, A. Léon, O. Zabara and M. Fichtner, *J. Mater. Chem.*, 2007, **17**, 3496.
18 P. Zanella, L. Crociani, N. Masciocchi and G. Giunchi, *Inorg. Chem.*, 2007, **46**, 9039.

19 Y. Filinchuk, B. Richter, T. R. Jensen, V. Dmitriev, D. Chernyshov and H. Hagemann, *Angew. Chem., Int. Ed.*, 2011, **50**, 11162.
20 M. Tamura and J. Kochi, *J. Organomet. Chem.*, 1971, **29**, 111.
21 M. Bremer, G. Linti, H. Nöth, M. Thomann-Albach and G. E. W. J. Wagner, *Z. Anorg. Allg. Chem.*, 2005, **631**, 683.
22 M. Bremer, H. Nöth and M. Warchhold, *Eur. J. Inorg. Chem.*, 2003, 111.
23 G. L. Soloveichik, M. Andrus and E. B. Lobkovsky, *Inorg. Chem.*, 2007, **46**, 3790.
24 R. Černý, N. Penin, V. D'Anna, H. Hagemann, E. Durand and J. Růžička, *Acta Mater.*, 2011, **59**, 5171.
25 V. D. Makhaev, A. P. Borisov, T. P. Gnilomedova, E. B. Lobkovskii and A. N. Chekhlov, *Bull. Acad. Sci. USSR Div. Chem. Sci.*, 1987, **36**, 1582.
26 V. D. Makhaev, A. P. Borisov, T. P. Karpova and L. A. Petrova, *Russ. J. Inorg. Chem.*, 1995, **40**, 1579.
27 V. D. Makhaev, Priv. Commun., 2014.
28 B. Richter, N. A. Tumanov, D. B. Ravnsbæk, Y. Filinchuk and T. R. Jensen, *Dalton Trans.*, 2015, **44**, 3988.
29 G. L. Soloveichik, M. Andrus, Y. Gao, J.-C. Zhao and S. Kniajanski, *Int. J. Hydrogen Energy*, 2009, **34**, 2144.
30 S. K. Sharov, L. P. Portnov, L. P. Ivanov and A. I. Gorbunov, *Russ. J. Phys. Chem.*, 1987, **61**, 1405.
31 H. C. Brown, Y. M. Choi and S. Narasimhan, *Inorg. Chem.*, 1982, **21**, 3657.
32 D. A. Brandreth and M. C. Molstad, *J. Chem. Eng. Data*, 1962, **7**, 449.
33 V. Mikheeva and E. Troyanovskaya, *Bull. Acad. Sci. USSR Div. Chem. Sci.*, 1971, **20**, 2497.
34 H. C. Brown, Y. M. Choi and S. Narasimhan, *Inorg. Chem.*, 1981, **20**, 4454.
35 H. I. Schlesinger, H. C. Brown, H. R. Hoekstra and L. R. Rapp, *J. Am. Chem. Soc.*, 1953, **75**, 199.
36 M. H. Jones, W. Levason, C. A. McAuliffe and M. J. Parrott, *J. Chem. Soc., Dalton Trans.*, 1976, 1642.
37 V. A. Abakshin, G. A. Krestov and O. V. Eliseeva, *J. Gen. Chem. USSR*, 1987, **57**, 1431.
38 A. V. Levkin and A. Y. Tsivadse, *Russ. J. Inorg. Chem.*, 1986, **31**, 161.
39 B. D. James and M. G. H. Wallbridge, *Prog. Inorg. Chem.*, 1970, **11**, 99.
40 D. Seebach, A. Thaler and A. K. Beck, *Helv. Chim. Acta*, 1989, **72**, 857.
41 H. C. Brown, S. Narasimhan and Y. M. Choi, *J. Org. Chem.*, 1982, **47**, 4702.
42 U. Mirsaidov, A. Kurbobekov and M. Khikmatov, *Russ. J. Inorg. Chem.*, 1981, **26**, 1538.
43 V. D. Makhaev and K. N. Semenenko, *Bull. Acad. Sci. USSR Div. Chem. Sci.*, 1978, **27**, 2520.
44 V. D. Makhaev, A. P. Borisov, N. G. Mozgina, G. N. Boyko and K. N. Semenenko, *Neorg. Mater.*, 1978, **14**, 1726.
45 R. Černý, G. Severa, D. B. Ravnsbæk, Y. Filinchuk, V. D'Anna, H. Hagemann, D. Haase, C. M. Jensen and T. R. Jensen, *J. Phys. Chem. C*, 2010, **114**, 1357.
46 D. B. Ravnsbæk, L. H. Sørensen, Y. Filinchuk, F. Besenbacher and T. R. Jensen, *Angew. Chem., Int. Ed.*, 2012, **51**, 3582.
47 T. Jaroń and W. Grochala, *Dalton Trans.*, 2010, **39**, 160.
48 T. Jaroń, W. Koźmiński and W. Grochala, *Phys. Chem. Chem. Phys.*, 2011, **13**, 8847.
49 T. Jaroń and W. Grochala, *Dalton Trans.*, 2011, **40**, 12808.
50 T. Jaroń, W. Wegner and W. Grochala, *Dalton Trans.*, 2013, **42**, 6886.
51 P. Panissod and M. Drillon, in *Magnetism: Molecules to Materials IV: Nanosized Magnetic Materials*, ed. J. S. Miller and M. Drillon, Wiley-VCH Verlag GmbH, Weinheim, 2003, p. 243.
52 R. Liu, D. Reed and D. Book, *J. Alloys Compd.*, 2012, **515**, 32.
53 A. W. Addison, R. T. Nageswara, J. Reedijk, J. van Rijn and G. C. Verschoor, *J. Chem. Soc., Dalton Trans.*, 1984, 1349.
54 M. J. Ingleson, J. P. Barrio, J. Bacsa, A. Steiner, G. R. Darling, J. T. A. Jones, Y. Z. Khimyak and M. J. Rosseinsky, *Angew. Chem., Int. Ed.*, 2009, **48**, 2012.
55 *CrysAlis PRO*, Agilent Technologies, 2013.
56 G. M. Sheldrick, *Acta Crystallogr., Sect. A: Found. Crystallogr.*, 2008, **64**, 112.
57 A. P. Hammersley, S. O. Svensson, M. Hanfland, A. N. Fitch and D. Hausermann, *High Pressure Res.*, 1996, **14**, 235.
58 A. Boultif and D. Louër, *J. Appl. Crystallogr.*, 2004, **37**, 724.
59 V. Favre-Nicolin and R. Černý, *J. Appl. Crystallogr.*, 2002, **35**, 734.
60 J. Rodríguez-Carvajal, *Phys. B*, 1993, **192**, 55.
61 G. Kresse and J. Furthmüller, *Phys Rev B: Condens. Matter*, 1996, **54**, 11169.
62 P. E. Blöchl, *Phys. Rev. B: Condens. Matter*, 1994, **50**, 17953.
63 J. P. Perdew, K. Burke and M. Ernzerhof, *Phys. Rev. Lett.*, 1996, **77**, 3865.
64 S. L. Dudarev, G. A. Botton, S. Y. Savrasov, C. J. Humphreys and A. P. Sutton, *Phys. Rev. B: Condens. Matter*, 1998, **57**, 1505.
65 C. Franchini, R. Podloucky, J. Paier, M. Marsman and G. Kresse, *Phys. Rev. B: Condens. Matter*, 2007, **75**, 195128.